Journal of Solid State Chemistry 184 (2011) 115–122

Contents lists available at ScienceDirect

Journal of Solid State Chemistry

journal homepage: www.elsevier.com/locate/jssc

Structure, thermal stability and properties of $Li_3Sc(BO_3)_2$

G.M. Cai [a,*], X.M. Tao [b], L.M. Su [a], F. Zheng [a], D.Q. Yi [a], X.L. Chen [c], Z.P. Jin [a,*]

[a] Science Center for Phase Diagram & Materials Design and Manufacture, Central South University, Changsha, Hunan 410083, PR China
[b] Department of Physics, Guangxi University, Nanning 530004, PR China
[c] Beijing National Laboratory for Condensed Matter Physics, Institute of Physics, Chinese Academy of Sciences, P.O. Box 603, Beijing 100080, PR China

ARTICLE INFO

Article history:
Received 7 May 2010
Received in revised form
15 October 2010
Accepted 31 October 2010
Available online 5 November 2010

Keywords:
Powder X-ray diffraction
Crystal structure
Electronic structure
Photoluminescence

ABSTRACT

Polycrystalline $Li_3Sc(BO_3)_2$ was synthesized through the solid-state reaction, which is air-, water- and thermal-stable below about 929 °C. Its crystal structure was resolved and refined on the basis of powder X-ray diffraction data. The metal–borate framework is built up from ScO_6 octahedra connected to each other by sharing common edges, corners and faces of BO_3 units and LiO_4 groups. Coordination surrounding of B–O in this structure, $[BO_3]^{3-}$ group, was confirmed by an infrared absorption spectrum of an $Li_3Sc(BO_3)_2$. According to the electronic structure calculated by first-principles calculations, an $Li_3Sc(BO_3)_2$ is an insulator with a wide indirect energy band gap of about 4.4 eV. Considering the facile synthesis, large band gap, and thermal stability and excellent Tb^{3+}-doped photoluminescence characteristics of this compound in general, it may be a good candidate as host of phosphors deposited on chip of the light-emitting diodes for white-color conversion.

1. Introduction

Borates have long been a focus of research for their rich crystal-structure types, wide transmittance spectra and wide band gaps [1–5]. Search for new laser host, nonlinear optical, luminescent, birefringent and thermal neutron detector materials in borates, attentions have been paid to A_2O–RE_2O_3–B_2O_3 (A=alkali metals, RE=rare earth elements) ternary systems. Many compounds with different structure types were discovered in those systems, such as $Li_6RE(BO_3)_3$ (RE=Nd–Yb) family [6,7], $LiRE_6O_5(BO_3)_3$ (RE=Pr–Tm) family [8], $Li_3RE_2(BO_3)_3$ (RE=Pr–Yb) family [9,10], $Li_3Gd(BO_3)_2$ [11], $Na_3Nd(BO_3)_2$ [12], $Na_3RE_2(BO_3)_3$ (RE=La, Sm) [13] and $K_3RE(BO_3)_2$ (RE=Y, Nd–Lu) [14] and so on. As one part of a project for search for new photoelectric functional materials, our group recently have made a systematic survey of the Li_2O–Sc_2O_3–B_2O_3 system, with the confirmation of the borate.

The synthesis and structure of an $Li_3Sc(BO_3)_2$ were firstly described by H. Sun (1989, Ph.D. Dissertation, Oregon State University). And then, single crystal of the title compound has been obtained by Mao et al. and its crystal structure was determined by single-crystal X-ray diffraction study [15]. In this work, the crystal structure of an $Li_3Sc(BO_3)_2$ has been investigated using powder X-ray diffraction data by the direct method. The comparison of structure types of compounds $M_3R(BO_3)_2$ (M=Li, Na, K; R=trivalent metal) was given in this paper. Infrared spectrum of the title compound was measured to confirm an existence of anionic groups. First-principles calculations for an electronic structure of an $Li_3Sc(BO_3)_2$ have been performed at T=0 K in order to understand its basic physical properties and give prediction for its potential applications.

Low energy consumption, long lifetime and low-carbon are among the most desired properties of light-emitting diodes (LEDs). The development of white LEDs determines the necessity of efficient tricolor phosphors excited by UV chips. However, recent fact in weaker emission intensity of commercial green and red phosphors compared to blue phosphors is not favorable for future commercial applications of these LEDs. It is very important to search for new efficient green and red phosphors, especially for low ultraviolet excited. To our knowledge, Tb^{3+} are often investigated and used as excitons for luminescence materials [16,17]. In our work, the Tb^{3+} doped $Li_3Sc(BO_3)_2$ phosphor exhibited an intense green emission under UV excited and may be a good candidate for green phosphors in the application of white LEDs.

2. Experimental

2.1. Synthesis, chemical analysis and X-ray powder diffraction

Undoped and doped borates were synthesized by standard solid-state reactions. Firstly, all stoichiometric mixtures of Li_2CO_3 (spectral reagent), Sc_2O_3 (analytical reagent), Tb_4O_7 (spectral reagent) and H_3BO_3 (analytical reagent) were finely ground into powders in a mortar of agate. Secondly, the mixtures were preheated in an Al_2O_3 crucible at 600 °C for 12 h to decompose

* Corresponding authors. Fax: +86 731 88876 692.
E-mail addresses: gmcai2002@163.com (G.M. Cai), jin@mail.csu.edu.cn (Z.P. Jin).

0022-4596/$ - see front matter © 2010 Elsevier Inc. All rights reserved.
doi:10.1016/j.jssc.2010.10.035

H_3BO_3 and Li_2CO_3, and naturally cooled to room temperature. Subsequently, they were reground and sintered at 760∼860 °C for 48 h. In all cases, care was taken to add an extra 0.2 mol% H_3BO_3 and 0.1 mol% Li_2CO_3 in order to offset the weight losses of B_2O_3 and Li_2O in the procedure of synthesis.

The chemical compositions of the samples were measured by inductively coupled plasma atomic emission spectrometry, using a Perkin-Elmer ICP/6500 spectrometer.

X-ray powder diffraction data were recorded on an X-ray diffractometer (Rigaku D/Max-2500) with Cu $K\alpha$ radiation and a diffracted-beam graphite monochromator operated at a power of 40 kV and 150 mA. Inorganic Crystal Structure Database (ICSD release 2010) and the Powder Diffraction File (PDF release 2008) were used for phase analysis of the samples. The data for crystal structure analysis of an $Li_3Sc(BO_3)_2$ were collected at room temperature in step scan mode with a step size 0.02° (2 Theta), counting time 2 s per step and 2 Theta range 5∼130°. More technical details were listed in Table 1.

2.2. Ab initio investigation of crystal structure

All the reflections of the compound $Li_3Sc(BO_3)_2$ can be well indexed on the basis of a monoclinic unit cell with lattice parameters a=4.7744(1) Å, b=5.9461(1) Å, c=9.3962(2) Å and β=119.36(1)° using the program DICVOL04 [18]. The systematic absence of h0l with $l=2n+1$, 0k0 with $k=2n+1$ and 00l with l=$2n+1$ suggests the possible space group is $P2_1/c$. In addition, there is no efficiency of second harmonic generation (SHG) in the powder sample of an $Li_3Sc(BO_3)_2$ using the Kurtz–Perry technique [19], which is consistent with centrosymmetric $P2_1/c$ space group.

The whole pattern of an $Li_3Sc(BO_3)_2$ was fit using the program FullProf_suite [20] based on the Le Bail method [21], and a total of 392 independent $|F_{obs}|$ values were extracted. Each unit cell contains 24 atoms, based on the lattice parameters and the density of the sample (D_m=2.568 g/cm^3), which was measured using METTLER TOLEDO by Archimedes' principle. Direct method was applied with SHELXL97 program package [22] to the extracted $|F_{obs}|$. According to the atom distances, four peaks listed in the E-map were likely to correspond the correct positions of four atoms, in which one was assigned to the Sc atom and the other was ascribed to the three O atoms. The other atoms, B atoms and Li atoms were located by using difference Fourier synthesis. During this course, once an atom was located, it would be used for next run of the difference Fourier synthesis. After a satisfactory rough structure was obtained, it was refined by the Rietveld method [23,24], using the program FullProf_suite. A total of 32 structural parameters and 13 profile parameters were refined, with the pseudo-Voigt function used as the peak shape function. The refinement finally converged to agreement factors of R_B=4.76%, R_P=9.89% and R_{WP}=12.8% with S=1.79. Lattice parameters were refined to be a=4.7766(1) Å, b=5.9452(1) Å, c=9.3958(2) Å and β=119.836(1)°. From the final refinement pattern shown in Fig. 1, the agreement between calculations and experiments of its powder XRD pattern is quite good. The crystallographic data of an $Li_3Sc(BO_3)_2$ are given in Table 1. Fractional atomic coordinates and equivalent isotropic displacement parameters are obtained by the Rietveld refinement (see Table 2). Some selected geometric parameters in the monoclinic structure of an $Li_3Sc(BO_3)_2$ are listed in Table 3.

Table 1
Details of Rietveld refinement and crystal data of an $Li_3Sc(BO_3)_2$.

Sample	Multi-crystal powder
Diffractometer	MXP21VAHF/M21X
Radiation type	Cu $K\alpha$
Monochromator	Graphite
Wavelength (Å)	1.5405
Refined profile range (°2θ)	5–130
Step size (°2θ)	0.02
Step scan time per step (s)	2
Number of structure parameters	32
Number of profile parameters	13
R_B	4.76%
R_P	9.89%
R_{WP}	12.8%
S	1.79
Formula	$Li_3Sc(BO_3)_2$
Symmetry	Monoclinic
Space Group (S.G.)	$P2_1/c$
A (Å)	4.7766(1)
B (Å)	5.9452(1)
C (Å)	9.3958(2)
B (°degree)	119.836(1)
Volume (Å^3)	231.45
Z	2
Measured density (g cm^{-3})	2.607
Calculated density (g cm^{-3})	2.631

2.3. IR spectra measurement

Infrared spectra in the 350∼2000 cm^{-1} wavenumber range were obtained by using a Perkin-Elmer 983G infrared spectrophotometer with KBr pellets as standards.

2.4. First-principles calculation

A first-principles study of the electronic structure for an $Li_3Sc(BO_3)_2$ was presented by using the scalar relativistic all-electron Bloch's projector augmented wave method within the generalized gradient approximation (GGA) [25,26], as implemented in the highly efficient Vienna ab initio simulation package (VASP) [27,28]. For the GGA exchange-correlation potential, the Perdew–Burke–Ernzerhof parameterization (PBE) [29] is employed. The k-point meshes for Brillouin zone sampling were constructed using the Monkhorst–Pack scheme [30], and the reciprocal space meshes are increased to achieve convergence to a precision of better than 1 meV/at. The plane-wave kinetic-energy cutoff is set as 600 eV for all calculations. We have optimized the structure by minimization of the forces acting on the atoms. Once the forces are minimized in this construction, one can then find the self-consistent density at these positions by turning off the relaxations and driving the system to self-consistency. We take

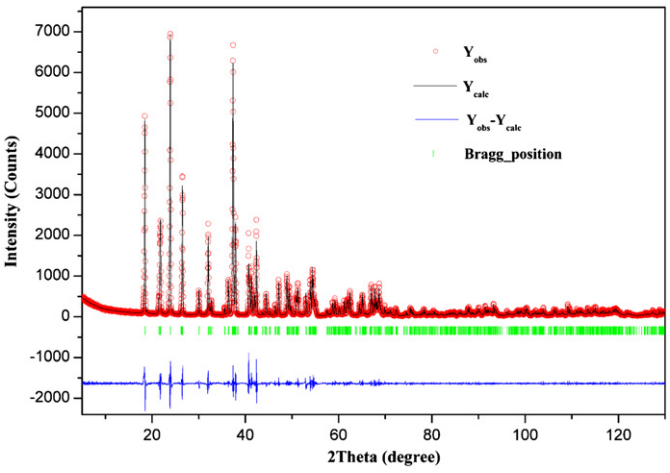

Fig. 1. Final Rietveld refinement patterns of $Li_3Sc(BO_3)_2$.

Table 2
Atomic coordinates and isotropic displacement parameters for an $Li_3Sc(BO_3)_2$.

Atom	site	X	y	Z	B (Å^2)
Sc1	2b	0	0	0	0.130(0)
O1	4e	−0.3124(1)	0.24432(6)	0.00299(5)	0.020(0)
O2	4e	0.3689(1)	0.08500(7)	0.24202(4)	0.020(0)
O3	4e	−0.1201(1)	−0.26665(6)	0.11015(4)	0.020(0)
Li1	2c	0	−1/2	0	0.034 (1)
Li2	4e	−0.3110(3)	0.2523(2)	0.2045(1)	0.034 (1)
B1	4e	0.3884(2)	0.1937(1)	0.37617(9)	−0.010(1)

Table 3
Selected geometric parameters (Å or °).

Atomic coordination		R	Atomic coordination		R
Sc(1)	–O(1)[a]	2.0926(5)	Li(1)	–O(3)	1.9788(4)
	–O(1)	2.0926(5)		–O(3)[b]	1.9788(4)
	–O(3)	2.1223(4)		–O(1)[a]	2.1400(5)
	–O(3)[a]	2.1223(4)		–O(1)[c]	2.1400(5)
	–O(2)	2.1317(3)	B(1)	–O(3)[d]	1.3705(12)
	–O(2)[a]	2.1317(3)		–O(2)	1.3778(10)
Li(2)	–O(1)	1.8906(13)		–O(1)[f]	1.3797(8)
	–O(3)[d]	1.9281(10)	O(3)[d] –B(1)–O(2)		121.716(66)
	–O(2)[e]	1.9969(15)	O(3)[d] –B(1)–O(1)[f]		119.223(75)
	–O(2)[d]	2.0928(13)	O(2)–B(1)–O(1)[f]		119.005(55)

[a] $-x,-y,-z$.
[b] $-x,-1-y,-z$.
[c] $x,-1+y,z$.
[d] $-x,0.5+y,0.5-z$.
[e] $-1+x,y,z$.
[f] $1+x,0.5-y,0.5+z$.

the full relativistic effects for core states and use the scalar relativistic approximation for the valence states.

2.5. Differential thermal analysis

The thermal stability was investigated by the differential thermal analysis. A WCR-DTA high-temperature differential thermal instrument was employed to perform DTA. Sample and alumina reference were enclosed in Al_2O_3 cups. The heating rate was 5 °C/min in a temperature range from room temperature to 1050 °C.

2.6. Fluorescence spectroscopy

The luminescence properties of Tb^{3+} doped samples were investigated by fluorescence emission and excitation spectra under an ultraviolet (UV) excitation. The fluorescence spectra were recorded by using a Hitachi F-7000 Fluorescence Spectrophotometer in a scanning range 200–700 nm. The obtained data were corrected for emission and excitation with respect to the Xe lamp excitation source.

3. Results and discussion

The atomic ratio of Li, Sc and B in the sample was near to 3:1:2, determined by an ICP atomic emission spectrometry.

3.1. Crystal structure

The structure of $Li_3Sc(BO_3)_2$ in the (*ac*) plane is depicted in Fig. 2, showing the bi-dimensional aspect for assembly of ScO_6 octahedra and planar BO_3 triangles. The ScO_6 octahedra constitute three layers parallel to the (*bc*) plane. The connection between two ScO_6 octahedra layers is ensured by the planar BO_3 anionic groups by common edges, corners running parallel to the (0 1 0) direction.

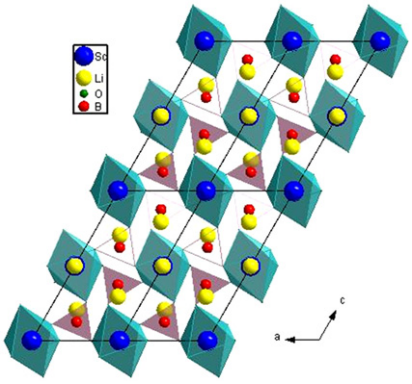

Fig. 2. Structure of an $Li_3Sc(BO_3)_2$ along the (0 1 0) direction. Large gray circles stand for Li atoms, small gray circles for B atoms, big black circles for Sc atoms and small black circles for O atoms.

Table 4
Bond valence analysis of an $Li_3Sc(BO_3)_2$.

Atoms	O(1)	O(2)	O(3)	Σs_{calc}	Σs_{theo}
Li(1)	0.16122 × 2		0.25027 × 2	0.82296	1
Li(2)	0.31619 × 1	0.23857 × 1	0.28701 × 1	1.02538	1
		0.18359 × 1			
Sc(1)	0.51755 × 2	0.46578 × 2	0.47776 × 2	2.9222	3
B(1)	0.97546 × 1	0.98021 × 1	0.99899 × 1	2.9547	3

Note: the results refer to the equation $s=\exp[(r_0-r)/B]$ with $r_0=1.466$, 1.849 and 1.371 Å for Li–O, Sc–O and B–O, respectively, and B = 0.37.

In the building units of $Li_3Sc(BO_3)_2$ structure, Li(1) species is located on position 2*c* and surrounded by four oxygen atoms with bond distances ranging 1.9788–2.1401 Å, forming irregular rectangles $Li(1)O_4$. Li(2) species are located on position 4*e* and coordinated to four oxygen atoms with bond distances ranging 1.8915–2.0921 Å. One Li(2) with one O(1), one O(3) and two O(2) atoms form irregular $Li(2)O_4$ tetrahedra, which connect each other parallel to the ab crystal plane by sharing vertexes, and interconnect with $Li(1)O_4$ rectangles along the *c* axis by sharing corners.

To examine validity of the determined structure of an $Li_3Sc(BO_3)_2$, Brown's bond valence method [31] was used to calculate the valence sum for each ion. Bond valence analysis of an $Li_3Sc(BO_3)_2$ is reported in Table 4. The results of the calculations indicate that the calculated valence sums for all ions are reasonable.

By the way, the difference of lattice parameters for an $Li_3Sc(BO_3)_2$ between our work and literature [15] are due to the different choices for unit cell. In fact, these two crystal structures have the same symmetrical characteristic.

3.2. IR spectra

In order to further confirm the coordination surroundings of B–O in the $Li_3Sc(BO_3)_2$ structure, an infrared absorption spectrum for $Li_3Sc(BO_3)_2$ was measured at room temperature and given in Fig. 3. Bands below 500 cm^{-1} mainly originates from the lattice dynamic modes, while the bands with maxima at about 700∼800 cm^{-1} should be attributed to the B–O out of plane bending vibration. According to the previous work [32], the strong absorption wavenumber profile above 1145 cm^{-1} is generated by the stretching vibrations of the triangular BO_3 groups. It is found that there are several closely spaced peaks about 1200 cm^{-1}, which are

believed to come from the different bond lengths of B–O. In a word, the IR spectrum for an $Li_3Sc(BO_3)_2$ confirm the existence of the $[BO_3]^{3-}$ groups.

3.3. Crystal structure of compounds $M_3R(BO_3)_2$ (M=Li, Na, K; R=trivalent metal)

Although the title compound has similar isolated planar $[BO_3]^{3-}$ anionic groups and the same formula $M_3R(BO_3)_2$ with $Li_3Al(BO_3)_2$, $Li_3In(BO_3)_2$ and $K_3RE(BO_3)_2$ (RE=Y, Nd–Lu), different structures are found in those orthoborates. Table 5 lists crystal informations of compounds $M_3R(BO_3)_2$ (M=Li, Na, K; R=Al, Ga, In, Sc, RE) reported in both previous literatures [11,12,14,33–38] and this work. From Table 1, one can see that symmetry of the compounds $M_3R(BO_3)_2$ becomes higher with an expansion of M' ionic radius [39]. In addition, unit cell expands linearly with the increasing of R' ionic radius. Most is worth mentioning, values for M^+/R^{3+} in $M_3R(BO_3)_2$ are between 0.7234 for $Li_3Gd(BO_3)_2$ and 1.5647 for $K_3Lu(BO_3)_2$, as shown in Fig. 6. In authors' opinion, there are still many possible derivatives of an $M_3R(BO_3)_2$ (see Fig. 4a), if the M^+/R^{3+} ratios are dominant in determining stability and symmetry of these structures. Of course, the existences of those derivatives need to confirm by experiments. From the point of rule for ionic radii ratios, there must exist upper and lower limits for an M^+/R^{3+} in those compounds. In order to determine the maximum and minimum of M^+/R^{3+} values, syntheses of other substituted derivatives remain to be investigated in the futural work, for example $M_3R(BO_3)_2$ (M=Li and R=La, Ce, Pr, Nd, Sm, Bi, Eu; M=Na and R=Al, Ga; M=K and R=Al, Ga, In).

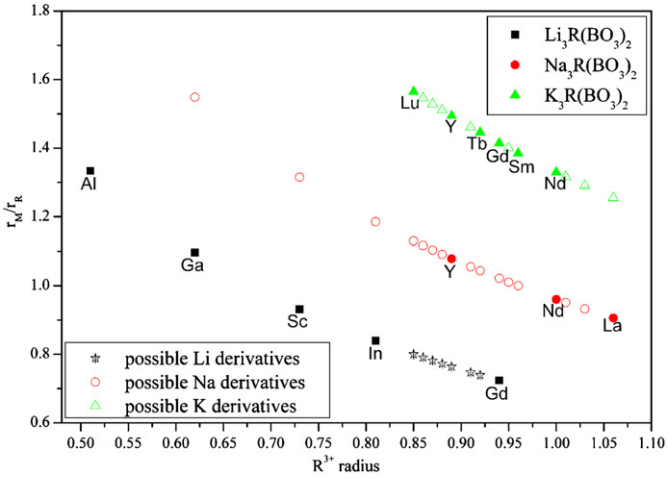

Fig. 4. The evolution of the ionic radii ratios M/R with increasing R^{3+} radius for $M_3R(BO_3)_2$ (M=Li, Na, K; R=trivalent metal) compounds.

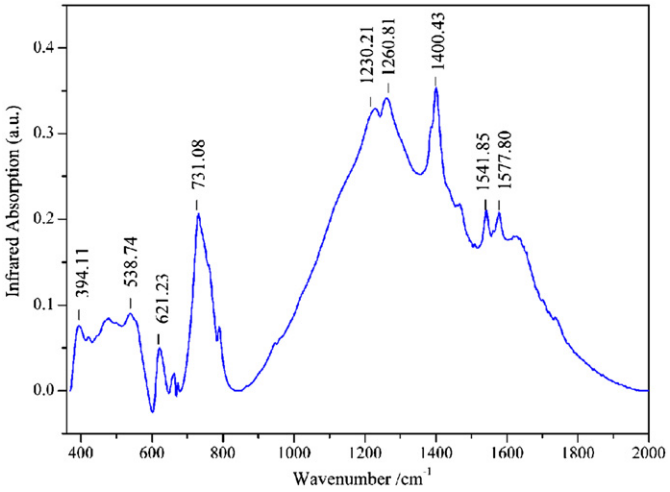

Fig. 3. Infrared spectra for an $Li_3Sc(BO_3)_2$.

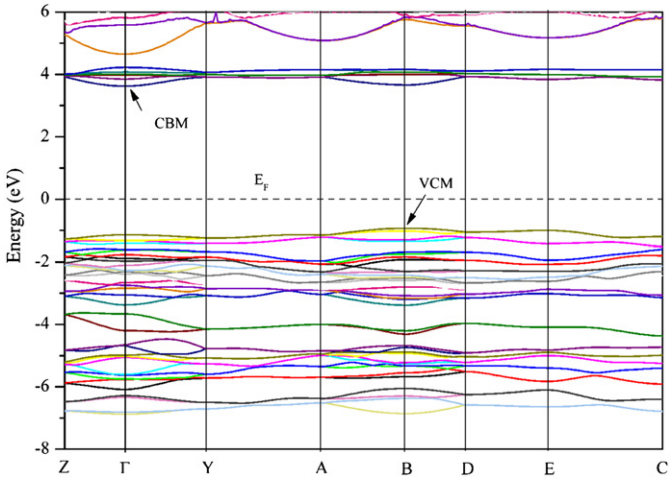

Fig. 5. The calculated band structure of an $Li_3Sc(BO_3)_2$.

Table 5
Crystal information of compounds $M_3R(BO_3)_2$ (M=Li, Na, K; R=Al, Ga, In, Sc, RE).

Compound	S. G.	a(Å)	b(Å)	c(Å)	β(°degree)	Z
[33]$Li_6Al_2(BO_3)_4$	P-1	6.131(2)	4.819(1)	8.227(3)	117.03(5)	1
[34]$Li_3Al(BO_3)_2$	P-1	4.876(8)	6.191(16)	7.910(20)	89.44(17)	2
[35]$Li_3Al(BO_3)_2$	P-1	4.88870(10)	6.17150(10)	7.88850(10)	89.54(3)	2
[36]$Li_6Ga_2(BO_3)_4$	P-1	6.23(3)	4.90(2)	8.42(5)	118.0(5)	1
$Li_3Sc(BO_3)_2$[a]	$P12_1/c1$	4.7766(1)	5.9452(1)	9.3958(2)	119.836(1)	2
[18]$Li_3Sc(BO_3)_2$	$P12_1/n1$	4.7831(17)	5.954(2)	8.163(3)	90.702(9)	2
[37]$Li_3In(BO_3)_2$	$P12_1/n1$	5.168(5)	8.899(9)	10.099(2)	91.112(1)	4
[11]$Li_3Gd(BO_3)_2$	$P12_1/c1$	8.724(2)	6.425(2)	10.095(2)	116.85(2)	4
[38]$Na_3Y(BO_3)_2$	$P12_1/c1$	6.5050(3)	8.5172(1)	12.0213(1)	118.73(7)	4
[12]$Na_3Nd(BO_3)_2$	$P12_1/c1$	6.618(5)	8.810(5)	12.113(5)	122.27	4
[14]$K_3Lu(BO_3)_2$	$Pnnm$	9.289(3)	6.768(5)	5.496(6)	90	2
[14]$K_3Y(BO_3)_2$	$Pnnm$	9.3377(9)	6.7701(6)	5.5058(4)	90	2
[14]$K_3Tb(BO_3)_2$	$Pnnm$	9.3413(5)	6.774(4)	5.510(9)	90	2
[14]$K_3Gd(BO_3)_2$	$Pnma$	9.010(17)	7.046(12)	11. 150(16)	90	4
[14]$K_3Sm(BO_3)_2$	$Pnma$	9.046(3)	7.100(2)	11.186(3)	90	4
[14]$K_3Nd(BO_3)_2$	$Pnma$	9.052(5)	7.146(4)	11.205(6)	90	4

[a] This work.

3.4. Band structure, density of states

Fig. 5 presented the calculated band structure (BS) of an $Li_3Sc(BO_3)_2$. It possesses an indirect energy band gap of about 4.4 eV determined by B point at maximum of valence bands (VBM) and *Z* point at minimum of conduction band (CBM). However, the real band gap for $Li_3Sc(BO_3)_2$ might be much larger, because GGA generally underestimates band gap of the 3*d* compound [40]. The large band gap will benefit accommodating both ground and excited states.

Total density of states (TDOS) along with Li–s/p, B–s/p, Sc–p/d and O–s/p partial (PDOS) are shown in Fig. 6. The electronic structure in an energy range from −20.0 to −17.0 eV originates predominantly from the B–s, O–s and Sc–p states. The electronic structure between −7.0 eV and Fermi energy (E_F) is mainly B–p and O–p states with small contributions of Li–s/p and Sc–p/d states. The significant contribution to the lower conduction band comes from the Sc–d, O–p, Li–s/p and B–p states. It is obvious that the Sc–d states in the conduction band have a dominant effect on the energy band gap dispersion. Although, the O–p states in the upper valence band and lower conduction band has an obvious effect on the energy band gap dispersion. The O–p character is concentrated in the upper valence band, with weak amounts in the conduction band.

Seen from the PDOS, Li–s/p hybridizing with O–p states around −20 up to 7 eV is observed. In the energy region around −20.0

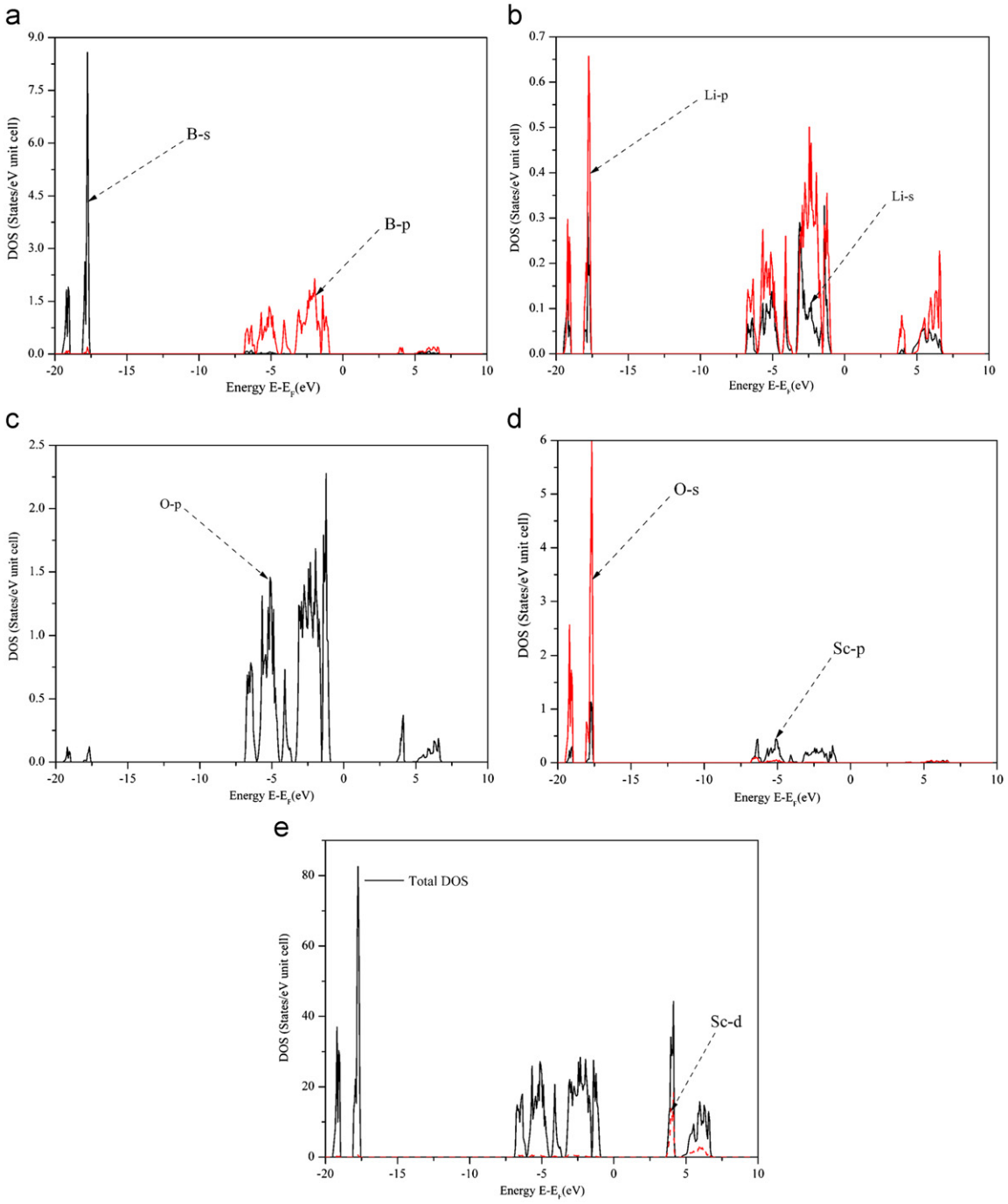

Fig. 6. (a–e) Calculated total and partial densities of states (states/eV unit cell) of an $Li_3Sc(BO_3)_2$.

up to −17 eV, O–s hybridizes with Sc–p and B–s states. In the energy region around −7.0 eV and above, O–p hybridized with B–p and Sc–p states. At the CBM, Sc–d hybridizes with O–p states. We find that the DOS extending from −7.0 eV up to an E_F is larger from O–p states (2.5 electrons/eV), B–p states (2.2 electrons/eV), Li–s/p states (0.3–0.5 electrons/eV) and Sc–p/d (0.3 electrons/eV). This is obtained by comparing the total densities of states with the angular momentum projected DOS of O–p, B–p, Li–s/p and Sc–p/d states as shown in Fig. 6. These results show that some electrons from O–p, B–p, Li–s/p and Sc–p/d states are transferred into valence bands (VBs) and contribute to weak covalence interactions of Li–O, Sc–O, Li–B and Sc–B atom pairs, and the substantial covalence interactions of B and O atoms. All the Li–O and Sc–O bonds are prevailingly of an ionic character, and for B–O bonds are of covalent character. It is concluded that the covalent strength of B–O bonds in the triangular $[BO_3]^{3-}$ units is stronger than that of Li–O and Sc–O bonds.

3.5. Thermal stability

With the solid-state reaction technique, three stoichiometric mixtures of Li_2CO_3, Sc_2O_3 and H_3BO_3 were preheated at 600 °C and sintered at 760, 820 and 860 °C, then cooled down to room temperature. The powder XRD patterns for those synthesized samples (Fig. 7) shows that pure $Li_3Sc(BO_3)_2$ phase can form at temperature range 760–860 °C. In order to study its thermal stability, three circled DTA curves for the pure $Li_3Sc(BO_3)_2$ were measured and shown in Fig. 8. Because there is neither endothermic nor exothermic peak below 700 °C, the range of DTA curves shown in Fig. 8 is from 700 to 1050 °C. Combined with experimental observation and XRD analysis, an $Li_3Sc(BO_3)_2$ decomposes along with volatilization at about 929 °C. The pure $Li_3Sc(BO_3)_2$ sample becomes fewer after treated at 930 °C for half an hour and air-quenching. Its products included $Li_3Al(BO_3)_2$ (PDF 53-1130), Sc_2O_3 (PDF 05-0629) and $Li_6B_4O_9$ (PDF 18-0721), given that part of products have reacted with an Al_2O_3 crucible leading to the formation of an $Li_3Al(BO_3)_2$. So, the sharp endothermic peak at about 929 °C on the first heating curve is ascribed to decomposing point of the compound $Li_3Sc(BO_3)_2$. As for the exothermic peak at about 750 °C on the cooling curves is related to the phase-formation of the compound $Li_3Sc(BO_3)_2$. In our experiment, the pure $Li_3Sc(BO_3)_2$ was quickly heated to 929 °C for 5 s, cooled to 750 °C for 2 h at a cooling rate of 5 °C/min, then with the furnace cooling to room temperature. The powder XRD pattern of that treated sample sees Fig. 9, which consists of dominating

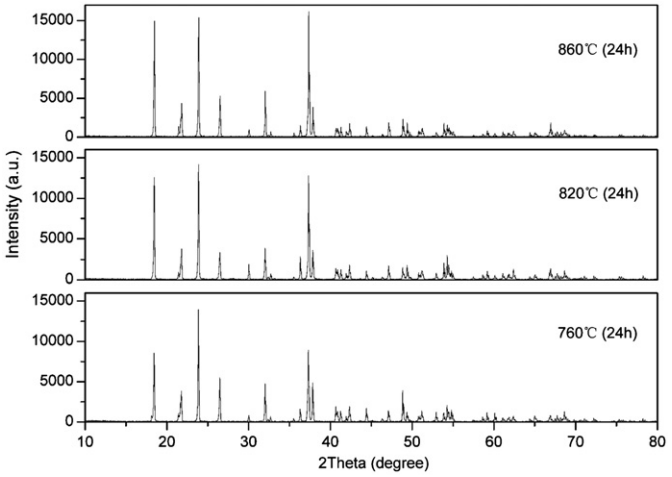

Fig. 7. The powder XRD patterns of products for the stoichiometric mixture of Li_2CO_3, Sc_2O_3 and H_3BO_3 sintered at 760, 820 and 860 °C, respectively.

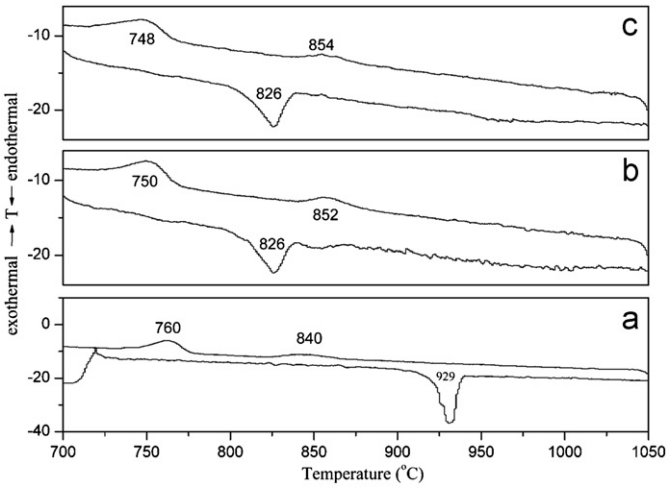

Fig. 8. Circular DTA curves for pure $Li_3Sc(BO_3)_2$: (a) Cycle 1: pure $Li_3Sc(BO_3)_2$ was quickly heated to 700 °C for 5 min, then heated to 1050 °C with a heating rate of 5 °C/min, kept for 5 s and cooled to 700 °C for 5 min with a cooling rate of 5 °C/min; (b) Cycle 2: the sample after cycle 1 was heated to 1050 °C with a heating rate of 5 °C/min, kept for 5 s and cooled to 700 °C for 5 min with a cooling rate of 5 °C/min; (c) Cycle 3: the sample after cycle 2 was heated to 1050 °C with a heating rate of 5 °C/min, kept for 5 s and cooled to 700 °C for 5 min with a cooling rate of 5 °C/min, then with the furnace cooling to room temperature.

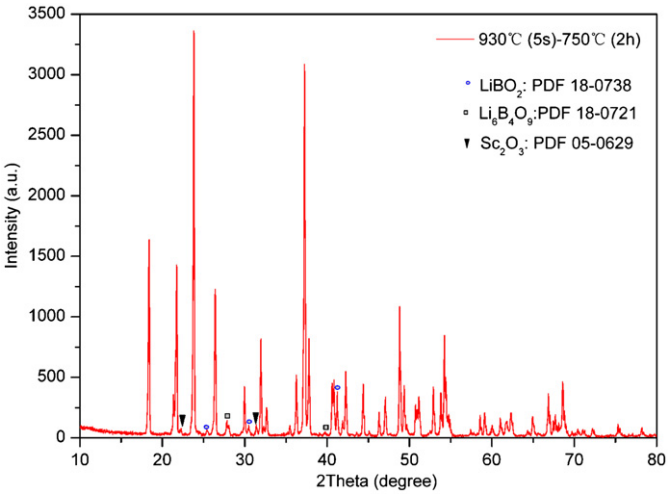

Fig. 9. Powder XRD pattern of the pure $Li_3Sc(BO_3)_2$ heat-treated by quickly heating to 930 °C for 5 s, cooled to 750 °C for 2 h with a cooling rate of 5 °C/min, then with the furnace cooling to room temperature.

$Li_3Sc(BO_3)_2$, a little $LiBO_2$ (PDF 18-0738), $Li_6B_4O_9$ (PDF 18-0721) and Sc_2O_3 (PDF 05-0629). It is suggested that the decomposed products of $Li_3Sc(BO_3)_2$ probably consist of $LiBO_2$, $Li_6B_4O_9$ and Sc_2O_3. From this point, the $Li_3Al(BO_3)_2$ is formed at about 929 °C through the reaction between an $LiBO_2$ and the Al_2O_3 crucible. And, the sharp endothermic peak at about 829 °C on the later two heating curves and the weak endothermic peak at about 840∼860 °C on the three cooling curves may well be the melting and freezing points for the binary compound $LiBO_2$ [41], respectively. In general, the DTA and experimental analysis shows that $Li_3Sc(BO_3)_2$ stabilizes below about 929 °C in air.

3.6. Luminescence characteristics of $Li_3Sc(BO_3)_2:Tb^{3+}$

The large band gap of $Li_3Sc(BO_3)_2$ inspires us to investigate photoluminescence property of this material with an incorporated

rare earth cation. Under 371 nm excitation, phosphor $Li_3Sc_{0.9}Tb_{0.1}(BO_3)_2$ emits a bright green color with the emission peaks located at 488, 498, 544, 548, 584, 592 and 622 nm, which is attributed to a group of typical $^5D_4 \rightarrow {}^7F_J$ ($J=6, 5, 4, 3$) transitions of Tb^{3+} ion with the predominant $^5D_4 \rightarrow {}^7F_5$ transition peaking at 544 nm (Fig. 10). From the point of the crystal structure, the surrounding situation of (Sc, Tb)O_6 octahedra can offer high-frequency vibrations mainly from BO_3 groups in the matrix $Li_3Sc(BO_3)_2$. As a result, the non-radiative relaxation to the $^5D_4$ is high and the $^5D_3$ emission is difficult to observe.

Weak bands peaking at 318, 341, 351, 358, 369, 376 and 485 nm and strong bands peaking at 358, 369 and 376 nm were observed in the excitation spectrum monitoring 544 nm emission (Fig. 11). The excitation spectra of Tb^{3+} consist of weak spin-allowed (SA) 4*f*–5*d* bands within 300–330 nm, strong spin-forbidden (SF) 4*f*–5*d* bands within 330–370 nm, and $^7F_6$–^5D_J ($J=3$, 4) transition peaks at around 376 and 485 nm [42]. It is an interesting phenomenon that this novel phosphor can strongly absorb ultraviolet (369 nm) suitable for the UV or blue output wavelengths of GaN-based LED chips [43,44].

Except facile synthesis, the polycrystalline $Li_3Sc(BO_3)_2$: Tb^{3+} is highly stable in air. What is more, the effective excitation wavelength for 369 nm is in good agreement with the emission wavelength of GaN-based LED chips. In general, chemical stabilization, relatively simple preparation and luminescent characteristics make $Li_3Sc(BO_3)_2$:Tb^{3+} can be a potential candidate of the phosphors deposited on LED-chip for color conversion.

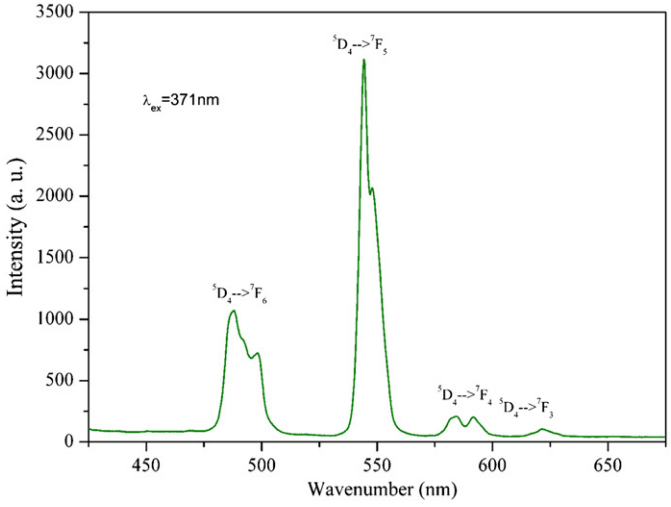

Fig. 10. UV emission spectra of an $Li_3Sc_{0.9}Tb_{0.1}(BO_3)_2$ at room temperature ($\lambda_{ex}=371$ nm). The intensities have been normalized.

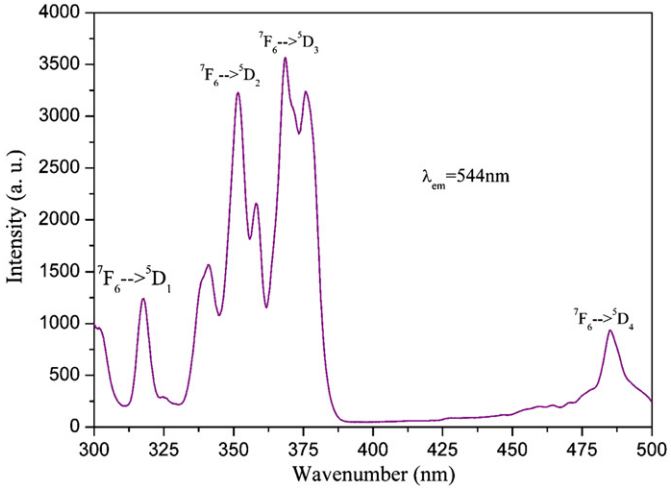

Fig. 11. UV excitation spectrum of an $Li_3Sc_{0.9}Tb_{0.1}(BO_3)_2$ monitoring the Tb^{3+} emission at 544 nm. The intensities have been normalized.

4. Conclusions

Pure $Li_3Sc(BO_3)_2$ powders were obtained at temperature range 760～860 °C through standard solid-state reaction, which are thermally stable below about 929 °C. Its crystal structure was reinvestigated by an ab initio method from powder X-ray diffraction data. The first-principles study of its electronic structure revealed that $Li_3Sc(BO_3)_2$ is an insulator with an indirect energy of about 4.4 eV. Angular momentum characters of each structure groups in its electronic structure were identified according to the PDOS. The nature of chemical bonding in this structure has been elucidated from its TDOS and PDOS. Phosphors $Li_3Sc(BO_3)_2$:Tb^{3+} can emit bright green light under the excitation of 369 or 376 nm. Chemical stabilization, relatively simple preparation, large quenching concentration and intense luminescence make phosphors $Li_3Sc(BO_3)_2$:Tb^{3+} have potential applications in an illumination area.

Acknowledgments

Financial support by the National Natural Science Foundation of China (Grant nos. 51002189 and 50872144) and Postdoctoral Grant of Central South University (Grant no. 761320470) is gratefully acknowledged. The authors thank Dr. Wen-Jun Wang and Yan-Ping Xu (*Institute of Physics, Chinese Academy of Science*) for XRD and PL measurements as well as Ph.D. Pei-sheng Wang and Prof. Yong Du (*State Key Laboratory for Powder Metallurgy, Central South University*) for DTA measurements.

References

[1] C.T. Chen, B.C. Wu, A.D. Jiang, G.M. You, Sci. Sin. B 28 (1985) 235.
[2] C.T. Chen, Y.C. Wu, A.D. Jiang, G.M. You, R.K. Li, S.J. Lin, J. Opt. Soc. Am. B 6 (1989) 616.
[3] L. Mei, X. Huang, Q. Wu, B. Wu, C. Chen, Z. Kristallogr. 210 (1995) 93.
[4] A.D. Mills, Inorg. Chem. 1 (1962) 960.
[5] R. Norrestam, M. Nygren, J.O. Bovin, Chem. Mater. 4 (1992) 737.
[6] G.K. Abdullaev, K.S. Mamedov, Russ. J. Inorg. Chem. 22 (1977) 389.
[7] J. Mascetti, C. Fouassier, P. Hagenmuller, J. Solid State Chem. 50 (1983) 204.
[8] J.P. Chaminade, P. Gravereau, V. Jubera, C. Fouassier, J. Solid State Chem. 146 (1999) 189.
[9] G.K. Abdullaev, K.S. Mamedov, I.R. Amiraslanov, A.I. Magerramov, Russ. J. Inorg. Chem. 18 (1977) 410.
[10] N.A. Akhmedova, A.A. Guseinova, N.M. Mustafaev, M.I. Zargarova, Russ. J. Inorg. Chem. 37 (1992) 1378.
[11] V. Jubera, P. Gravereau, J.P. Chaminade, Solid State Sci. 3 (2001) 469.
[12] J. Mascetti, M. Classe, C. Fouassier, J. Solid State Chem. 39 (1981) 288.
[13] G.C. Zhang, Y.C. Wu, P.Z. Fu, Chem. Lett. 5 (2001) 455.
[14] J.H. Gao, R.K. Li, Solid State Sci. 10 (2008) 26.
[15] L.Z. Miao, T.Y. Zhou, N. Ye, Acta Crystallogr. E 64 (2008) i38.
[16] C.J. Duan, H.H. Chen, X.X. Yang, J.T. Zhao, Opt. Mater. 28 (2006) 956.
[17] H.B. Liang, Q. Su, Y. Tao, J.H. Xu, Y. Huang, Mater. Res. Bull. 41 (2006) 1468.
[18] A. Boultif, D. Louer, J. Appl. Crystallogr. 37 (2004) 724.
[19] S.K. Kurtz, T.T. Perry, J. Appl. Phys. 39 (1968) 3798.
[20] J. Rodriguez-Carvajal, FullProf (Version 3.5d Oct98-LLB-JRC).
[21] A. Le Bail, H. Duroy, J.L. Fourquet, Mater. Res. Bull. 23 (1988) 447.
[22] G.M. Sheldrick, SHELXS97 and SHELXL97, University of Gottingen, Gottingen, Germany, 1997.
[23] H.M. Rietveld, Acta Crystallogr. 22 (1967) 151.
[24] H.M. Rietveld, J. Appl. Crystallogr. 12 (1979) 483.
[25] P.E. Blochl, Phys. Rev. B 50 (1994) 17953.
[26] G. Kresse, J. Joubert, Phys. Rev. B 59 (1999) 1758.
[27] G. Kresse, J. Furthmuller, Phys. Rev. B 54 (1996) 11169.
[28] G. Kresse, J. Furthmuller, Comput. Mater. Sci. 6 (1996) 15.
[29] J.P. Perdew, S. Burke, M. Ernzerhof, Phys. Rev. Lett. 77 (1996) 3865.
[30] H.J. Monkhorst, J.D. Pack, Phys. Rev. B 13 (1972) 5188.
[31] I.D. Brown, D. Altermatt, Acta Crystallogr. Sect. B 41 (1985) 244.

[32] E.I. Kamitsos, M. Karakassides, G.D. Chryssikos, J. Phys. Chem. 91 (1987) 1073.
[33] G.K. Abdullaev, Kh.S. Mamedov, Kristallografiya 27 (N) (1982) 381–383.
[34] M. He, X.L. Chen, V. Gramlich, C. Baerlocher, T. Zhou, B.Q. Hu, J. Solid State Chem. 163 (2002) 369–376.
[35] H.X. Wang, W.D. Cheng, D.G. Chen, H. Zhang, D.S. Wu, Y.J. Gong, Chin. J. Chem. 22 (2004) 232–237.
[36] G.K. Abdullaev, Kh.S. Mamedov, Zh. Strukt. Khim. 13 (1972) 943–946.
[37] N. Penin, M. Touboul, G. Nowogrocki, Solid State Sci. 3 (2001) 461–468.
[38] Y. Zhang, X.L. Chen, J.K. Liang, T. Xu, J. Alloys Compd. 333 (2002) 72–75.
[39] R.D. Shannon, C.T. Prewitt, Acta Crystallogr. B 25 (1969) 925;
R.D. Shannon, C.T. Prewitt, Acta Crystallogr. A 32 (1976) 751.
[40] P. Dufek, P. Blaha, K. Schwarz, Phys. Rev. B 50 (1994) 7279.
[41] B.S.R. Sastry, F.A. Hummel, J. Am. Ceram. Soc. 41 (1958) 7.
[42] F.S. Liu, Q.L. Liu, J.K. Liang, J. Luo, L.T. Yang, G.B. Song, Y. Zhang, L.X. Wang, J.N. Yao, G.H. Rao, J. Alloys Compd. 425 (2006) 278.
[43] I. Akasaki, H. Amano, K. Itoh, N. Koide, K. Manabe, Inst. Phys. Conf. Ser. 129 (1992) 851.
[44] I. Akasaki, H. Amano, Jpn. J. Appl. Phys. 36 (1997) 5393.